ACS APPLIED MATERIALS & INTERFACES
Research Article
www.acsami.org

First-Principles Analysis of Defect Thermodynamics and Ion Transport in Inorganic SEI Compounds: LiF and NaF

Handan Yildirim,[†,§] Alper Kinaci,[‡,§] Maria K. Y. Chan,[‡] and Jeffrey P. Greeley*,[†]

[†]School of Chemical Engineering, Purdue University, West Lafayette, Indiana 47907, United States
[‡]Center for Nanoscale Materials, Argonne National Laboratory, Argonne, Illinois 60439, United States

Supporting Information

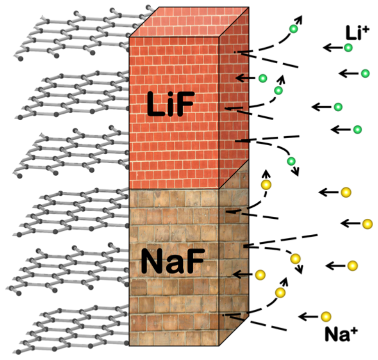

ABSTRACT: The formation mechanism and composition of the solid electrolyte interphase (SEI) in lithium ion batteries has been widely explored. However, relatively little is known about the function of the SEI as a transport medium. Such critical information is directly relevant to battery rate performance, power loss, and capacity fading. To partially bridge this gap in the case of inorganic SEI compounds, we report herein the results of first-principles calculations on the defect thermodynamics, the dominant diffusion carriers, and the diffusion pathways associated with crystalline LiF and NaF, which are stable components of the SEI in Li-ion and Na-ion batteries, respectively. The thermodynamics of common point defects are computed, and the dominant diffusion carriers are determined over a voltage range of 0−4 V, corresponding to conditions relevant to both anode and cathode SEI's. Our analyses reveal that for both compounds, vacancy defects are energetically more favorable, therefore form more readily than interstitials, due to the close-packed nature of the crystal structures. However, the vacancy concentrations are very small for the diffusion processes facilitated by defects. Ionic conductivities are calculated as a function of voltage, considering the diffusion carrier concentration and the diffusion barriers as determined by nudged elastic band calculations. These conductivities are more than ten orders of magnitude smaller in NaF than in LiF. As compared to the diffusivity of Li in other common inorganic SEI compounds, such as Li_2CO_3 and Li_2O, the cation diffusivity in LiF and NaF is quite low, with at least three orders of magnitude lower ionic conductivities. The results quantify the extent to which fluorides pose rate limitations in Li and Na batteries.

KEYWORDS: *solid electrolyte interface, LiF, NaF, DFT, defect thermodynamics, diffusion*

1. INTRODUCTION

Energy storage, which is among the most promising routes to mitigating dependence on fossil fuels, pollution, and climate change, has attracted increasing attention in the last few decades. Both Li-ion and beyond Li-ion battery (LIB) systems are plausible technologies for powering the next generation electric vehicles (EVs).[1] An interesting alternative to Li as the shuttle ion is Na. Na-ion batteries (NIBs) offer lower gravimetric/volumetric capacities compared to LIBs, yet the abundance of Na metal is a clear advantage for large-scale stationary applications.[2] For both LIBs and NIBs, significant challenges remain for enabling the large-scale commercialization needed for either plug-in hybrid electric vehicles (PHEVs) and full electric vehicles (EVs) or for backup power systems.[2] These batteries are generally comprised of a Li (Na)-containing positive electrode, a negative electrode, and an organic solvent-based electrolyte. Although the high voltages of LIBs and NIBs can yield substantial energy storage, these high voltages can also lead to side reactions at the interfaces between electrodes and electrolyte.[3] These interfacial reactions result from the fact that, under operating conditions, the common carbonate-based nonaqueous electrolytes, such as ethylene carbonate (EC) and dimethyl carbonate (DMC), are thermodynamically unstable. The electrolyte decomposition products react with the surfaces of electrodes (such as graphite, lithium, or silicon as negative electrodes), leading to formation of a thin film called a solid electrolyte interphase (SEI) layer. The electrode surface is coated with this layer during the first few charging cycles of the electrochemical cell. Both the presence and the nature of this SEI layer play a significant role in the stability and overall performance of LIBs and NIBs.[4−7] Cycling the battery below the reduction voltage of the electrolyte requires that the SEI layer be mechanically stable to electronically isolate the electrode from the electrolyte and to conduct ions,[8,9] thereby permitting alkali ion transport to the electrode.[10] If the passage of electrons is not blocked by the SEI, this layer grows due to the continuous reduction of electrolyte-consuming carrier ions, thus reducing the battery capacity. On the other hand, if ionic transport from electrolyte to the electrode is inefficient, cell impedance will increase. These types of failure will result in battery degradation.[11,12]

Deficiencies in the SEI can lead to irreversible capacity loss, power fade, and reduced durability and safety.[13] To alleviate these problems, intense research efforts have been devoted to

Received: April 2, 2015
Accepted: August 10, 2015
Published: August 10, 2015

DOI: 10.1021/acsami.5b02904
ACS Appl. Mater. Interfaces 2015, 7, 18985−18996

understanding the SEI. In particular, its structure and composition have been explored using many experimental techniques, including X-ray photoelectron spectroscopy (XPS), infrared spectroscopy (IR), nuclear magnetic resonance (NMR) spectroscopy, and transmission electron microscopy (TEM).[14−16] The composition of the electrochemically formed SEI layer on the negative electrode in LIBs, with a standard electrolyte solution of $LiPF_6$ salt in carbonate solvents such as ethylene and dimethyl carbonates, is a mixture of organic compounds containing EC reduction products (lithium ethylene dicarbonate $(CH_2CO_3Li)_2$[10,17] and ROLi, where R is an organic group that depends on the solvent) in an outer layer near the SEI/electrolyte interface, and inorganic materials (e.g., Li_2CO_3, LiF, and Li_2O)[18] in an inner layer near the SEI/electrode interface.[8,19] Other frequently reported components include CH_3OCO_2Li, $CH_3CH_2OCO_2Li$, CH_3OLi, CH_3CH_2OLi, $LiOCH_2CH_2OLi$, and $Li_xPF_yO_z$.[20] For example, it was reported for graphite electrodes that, after the first charge, EC molecules are decomposed and form a 3−10 nm thick SEI layer, which consists of Li_2CO_3, $(CH_2CO_3Li)_2$, and the products of salt decomposition.[9] In another study for graphite anodes, with an electrolyte composed of $LiPF_6$/EC, the SEI layer has been reported to be composed of $(CH_2CO_3Li)_2$, LiF, and low concentrations of $Li_xPF_yO_z$.[18] In a recent study by Salas et al.,[21] the progression of SEI layer formation on hydrogenated amorphous Si was determined as a function of applied potential during the first charge by combining cyclic voltammetry (CV) measurements with surface chemical analysis. After the initial lithiation, the SEI layer was reported to be mainly composed of LiF, along with low concentrations of $LiPF_6$, Li_xPF_y, and PF_y.[21] In comparison with the vast literature on anode SEI's in LIBs, there are relatively few characterization studies for NIBs. Komaba et al.[16] studied the SEI on hard carbon anodes using $NaClO_4$ with propylene carbonate (PC) electrolyte in a NIB. They reported a nonuniform SEI layer with possibly more inorganic compounds compared to an LIB with the same configuration. On the other hand, PC solutions with $NaPF_6$ or $NaN(SO_2CF_3)_2$ showed better cyclic performance compared to $NaClO_4$. Further, the use of fluorine-containing salts/additives has generally been shown to improve NIB performance with EC and PC solvents.[7]

While at lower voltages, electrolyte reduction on the negative electrode is common, oxidation at the cathode is possible at higher voltages. Although much less is known about the composition of the SEI on cathodes, on the surfaces of $Li_xMn_2O_4$ and Li_xCoO_2, products such as LiF,[22] acetone,[23] aldehydes,[24] CO_2,[24] organic radicals,[25] and carboxylic acid species[26] have been reported. As is the case with the anode SEI, the use of $LiPF_6$ salts has been suggested to lead to the formation of fluorine-containing compounds, which are believed to slow Li ion transport to the cathode.[22]

Even after its formation during the initial charging cycles, the SEI layer is often dynamic and evolves over the battery's lifetime. The changes in its chemical, mechanical, electronic, and ion transport properties, in turn, have a direct effect on battery performance. Even though many efforts have been made to improve the stability of the SEI layer, very little is known about the degradation mechanism, the underlying reasons for the changes in the conductivity, and how alkali ions are transported within the SEI. Many theories about the latter phenomenon, such as ion transport via porous regions, via grain boundaries between the SEI components, or via interstitials and vacancies, have been advanced, and such transport behavior is likely specific to each SEI component. Some experimental diffusion coefficients from the analysis of the electrochemical impedance spectroscopy data[27] are available although it is quite challenging to measure ion diffusion in the thin heterostructured SEI layer. Thus, computational studies are invaluable to provide such atomic-level details. This information, in turn, is important for understanding the relationship between the SEI and the properties of the battery as a whole because earlier studies suggested that Li ion diffusion through the SEI layer is rate limiting for the overall charge-transfer reaction.[28]

While ion transport in electrolytes has received significant attention using a variety of methods, including molecular dynamics (MD) studies,[29,30] ab initio simulations,[31] quantum chemistry calculations,[32,33] and charge transport in electrodes[34] and coating materials,[35] SEI compounds themselves have been considered in only a relatively small number of theoretical studies. Using density functional theory (DFT) calculations, Iddir et al.[36] investigated Li ion diffusion barriers in crystalline Li_2CO_3, which is often considered to be a majority component of SEIs formed from carbonate-based electrolytes.[20] The authors reported slow diffusion across the planes of Li_2CO_3 (0.60 eV), while smaller migration barriers (0.28 eV) were found along the open channels in the [010] directions. More recently, Shi et al.[4] used a combination of experiments and DFT calculations to determine the Li ion diffusion carriers and associated diffusion mechanisms in crystalline Li_2CO_3. The authors considered all relevant point defect energies in bulk Li_2CO_3, and they showed that the dominant diffusion carriers in Li_2CO_3 below 0.98 V are the Li-ion interstitials (Li_i^+), while above 3.98 V Li-ion vacancies become the dominant diffusion carriers. The interstitial Li_i^+ was shown to diffuse through a knock-off mechanism by continuously displacing the Li^+ in neighboring sites.[37]

The above studies are examples of the use of simple models of individual SEI compounds to obtain fundamental insights into the behavior of targeted regions of the SEI. Another often-reported inorganic compound in the SEI, which is also a natural subject for such fundamental studies, is LiF. Experimental observations, discussed above, suggest that this compound is observed on both graphite and Si negative electrodes. An experimental study also reported that the thermal stability of SEI's is related to the amount of LiF present.[38] For these reasons, LiF for LIBs, and the analogous compound NaF for NIBs, are important materials for the study of Li^+ and Na^+ transport through the inorganic SEI layer. However, to date, to our best knowledge, there are no studies reporting a complete analysis of charge carriers, diffusion mechanisms, and the associated barriers in both NaF and LiF. An earlier study[39] for bulk LiF reported a Li^+ diffusion barrier of 0.80 eV for a single vacancy diffusion mechanism. Another DFT study of the vacancy-assisted diffusion in bulk LiF reported the diffusion barrier to be 0.73 eV.[40] Experimentally obtained diffusion barriers, via NMR and conductivity measurements, were reported to be in the range of 0.65−0.73 eV.[41]

In the present study, we use periodic DFT calculations to provide a comprehensive, atomic-level analysis of the defect thermodynamics and ion diffusion characteristics of bulk LiF and NaF. Our theoretical approach combines thermodynamic analysis of relevant point defects in both structures to determine the dominant diffusion carriers, the densities of states (DOS) and band gaps, and diffusion barriers through the nudged elastic band (NEB) method. The defect concentrations are combined with the kinetic barriers to estimate net ionic conductivities for different defect types for both LiF and NaF.

This report is organized as follows. In section 2, we report on the details of the computational methods. In section 3, we provide the results and discussions. We discuss the details of the electronic structures of LiF and NaF, including the DOS and the band gaps, in section 3.1. In section 3.2, we give details on the defect formation energies and the concentrations in LiF and NaF. In section 3.3, we provide ion transport details in both structures from the NEB calculations. Finally, in section 4, we present the conclusions and discussions.

2. COMPUTATIONAL DETAILS

2.1. Details of the DFT Calculations. We employ first principles calculations to evaluate defect formation energies and diffusion barriers in bulk LiF and NaF. DFT calculations are performed with the projector augmented wave (PAW) method as implemented in the Vienna Ab-initio Simulation Package (VASP).[42] The generalized gradient approximation (GGA) with the parametrization of Perdew−Burke−Ernzerhof (PBE)[43] is used for the exchange correlation energy of interacting electrons. The energy cutoff for the planewave basis is 500 eV for LiF and 800 eV for NaF (the PAW potential for Na includes the semicore 2s and 2p states, and therefore requires a substantially larger planewave cutoff than the Li PAW potential). A 5 × 5 × 5 Monkhorst−Pack k-point mesh for both LiF and NaF is employed. The computational cells contain 64 atoms (2 × 2 × 2 cell, for NEB calculations) to 216 atoms (3 × 3 × 3 cell, for defect formation energy calculations). All calculations are performed spin-polarized. The convergence on the final forces is set at 0.01 eV/Å. For calculations involving charged defects, the total number of electrons in the supercell is adjusted accordingly for the excess charge introduced by the types of defects. For instance, to simulate a positively/negatively charged vacancy defect, one electron is removed/added to the supercell. A jellium background charge is introduced to maintain charge neutrality.[44]

2.2. Calculation of Defect Formation Energies and Defect Concentrations. The formation energy, $\Delta H_{d,q}$, of a defect, d, in charge state q is calculated from eq 1:[45]

$$\Delta H_{d,q}(E_F, \{\mu_i\}) = E_{d,q} - E_0 - \sum_i n_i\mu_i + q(E_V + E_F) \tag{1}$$

where $E_{d,q}$ is the total energy of supercell with defect d in charge state q, E_0 is the total energy of the pristine supercell, and μ_i and n_i are the chemical potential of the atomic species of the i^{th} defect and the corresponding number of atoms added to or removed from the structure. In the case of a vacancy defect (i.e., a removed atom), the sign of the n_i is negative. On the other hand, if the defect is an interstitial (i.e., an added atom), this sign is positive. In an operating electrode, the chemical potentials of the cations (μ_{Li} and μ_{Na}) range from close to the elemental limit to approximately 4 eV per atom below, as given by the voltage range with respect to Li/Li$^+$ (Na/Na$^+$). The chemical potential of fluorine is defined with respect to the cation chemical potential such that $\mu_F = E_0^{Li(Na)F} - \mu_{Li(Na)}$. The assumption involved with this description is that Li(Na)F is stable, which dictates the equality. Because the only source of F is from the irreversible decomposition of the Li(Na)PF$_6$ salt, there is no direct voltage control of the F chemical potential after the initial SEI formation.

The rightmost term in eq 1 represents the energy required to introduce a charge at the Fermi level. Accordingly, E_V represents the energy of the valence band maximum (VBM) and E_F is the Fermi level, which is referenced to the VBM. Before calculating the formation energies of the defects, we apply two corrections to the total energies of the defected structures. The first is the Makov−Payne[46] correction for the spurious image charge interactions between the jellium and added charge. The monopole term of the Makov−Payne correction, as cited in ref 46 is given by $\Delta E = q^2\alpha/\varepsilon L$, where α is the Madelung constant, ε is the dielectric constant, and L is the size of the simulation box. For ε, we consider two possible values: (1) the experimental static dielectric constant (ε_{static}), and (2) the electronic contribution to the dielectric constant ($\varepsilon_{electronic}$), calculated from density functional perturbation theory (DFPT). The detailed results for $\varepsilon_{electronic}$ are reserved for the Supporting Information, although selected values are reported in the main text. Second, we shift the electrostatic potential of the defected cells so that the local Hartree potential at points far away from the defect is realigned to the pristine value.[47]

It is necessary to obtain defect formation energies of defect groups such as Schottky defects without any defect−defect interactions as reference energies. However, determining noninteracting energies, particularly for multidefect supercell calculations, is often challenging and requires very large super cells, as was shown in an earlier study for Mg interstitials in MgO.[48] We note that the size of the supercell used in our study, (3 x 3 x 3), corresponds to 216-atom cell. To estimate the sensitivity of formation energies to the changes in the unit cell size, we also calculated $\Delta E = E_{d_g} - E_0$ for neutral and positively charged fluorine vacancies in (4 x 4 x 4) LiF supercells containing 512 atoms. For the neutral vacancy, the difference between $\Delta E_{4\times4\times4}$ and $\Delta E_{3\times3\times3}$ was found to be 5 meV. For the positively charged vacancy, modestly larger changes were found due to the Makov−Payne correction. We determined that when electronic contributions to ε are used to scale the monopole correction, the difference between $\Delta E_{4\times4\times4}$ and $\Delta E_{3\times3\times3}$ is 100 meV. This error drops slightly, to 60 meV, if the static dielectric constant is used. Thus, on the basis of these observations and the relatively large formation energies of the defects (discussed in section 3), we conclude that the size of the supercell used in our study should be sufficient to describe trends, and using larger size supercells is expected to lead to only modest quantitative changes in our conclusions.

For each set of elemental chemical potentials and temperatures, the Fermi energy of the system can be found by requiring charge neutrality, which is satisfied by requiring that the sum of charge density contributions from defects of type d and charge q ($c_{d,q}$), holes (h), and electrons (e) in the system equal zero, that is

$$Q = \sum_{d,q} qc_{d,q} + h - e = 0 \tag{2}$$

The concentration of any defect is derived from the formation energy by

$$c_{d,q}(E_F, \{\mu_i\}, T) = N_d \exp\left[-\frac{\Delta H_{d,q}(E_F, \{\mu_i\})}{k_B T}\right] \tag{3}$$

where N_d is the number of sites in which defects of type d can be realized in the system, k_B is the Boltzmann constant, and T is the temperature. The number of electrons and holes can be found by integrating over the conduction (from the conduction band minimum, E_C) and valence bands (up to the valence band maximum, E_V) in the electronic density of states of the pristine bulk material ($g(E)$) according to the Fermi distribution:

$$h - e = \int_{-\infty}^{E_V} [1 - f(E_F, T)]g(E)dE - \int_{E_C}^{\infty} f(E_F, T)g(E)dE \tag{4}$$

Equations 1 and 2 can be solved self-consistently at a fixed temperature (300 K in this study) to determine the Fermi level in the system. Once the E_F is determined, the formation energies and the concentrations of the defects can be calculated from eqs 1 and 3, respectively.

2.3. Nudged Elastic Band (NEB) Calculations. To determine the diffusion barriers associated with point defects, we perform NEB calculations[49] using three images. Test calculations performed using five images converge to the same transition state geometry and diffusion barrier. To account for the possibility that some metastable defects might have very low diffusion barriers and thus contribute to the overall ionic conductivity, we perform calculations for multiple diffusion mechanisms, including vacancy diffusion, interstitial diffusion via a direct-hopping mechanism (between the empty lattice sites), a knock-off mechanism (diffusion by displacing the ion to the neighboring lattice site), and a vacancy coupled diffusion mechanism. These mechanisms are evaluated, in select cases, for both neutral and charged defects. In addition to the diffusion carriers associated with the point defects in each structure, we have also evaluated the diffusion barriers for all defect types including the vacancies, the interstitials, and the vacancy pair point defects.

3. RESULTS AND DISCUSSION

3.1. Electronic Structures of LiF and NaF. Both LiF and NaF have a rocksalt structure, $Fm\bar{3}m$ (space group no. 225). The calculated lattice parameters are in good agreement with experimental values, with errors of 2.5−2.7% (Table 1).[50]

Table 1. Calculated Lattice Parameters and Band Gaps for LiF and NaF Using GGA-PBE[a]

structures	lattice parameters (Å)	band gaps (eV)
LiF	4.068 (4.068)[50] [3.964][50]	8.70 (9.24)[52] [13.7−14.2][51]
NaF	4.698 (4.709)[50] [4.579][50]	6.10 (6.06)[52] [11.5−11.7][51]

[a] Other theoretical (in parentheses) and experimental (in brackets) values obtained from the literature are also presented for comparison.

These highly ionic, closely packed crystals have very wide band gaps with experimentally reported values of 13.7−14.2 eV for LiF[51] and 11.5−11.7 eV for NaF.[51] Our GGA-PBE calculations underestimate the bands gaps (8.7 eV for LiF and 6.1 eV for NaF), as would be expected for DFT calculations using local and semilocal functionals. The total electronic densities of states (DOS) presented in Figure 1a,b for LiF and NaF show the strong insulating nature, indicating that the dense and compact inorganic part of the SEI is highly unfavorable for electronic conduction. We should, however, note that defects could substantially modify the electronic structure.

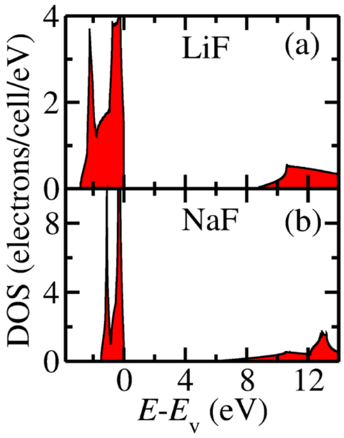

Figure 1. DFT computed total electronic density of states (DOS) for (a) LiF and (b) NaF. Valence band maxima (E_v) are set to zero in both cases.

To obtain the contributions from the holes and electrons to the total charge in eq 4, we used the electronic densities of states with one modification in which the conduction bands are rigidly shifted to extend the band gaps to the experimental values. The reason for such a modification is that, after self-consistent solution of eqs 1−4, it may be possible to obtain Fermi levels close to the conduction bands due to the substantially underestimated band gaps of GGA-PBE. Because of this shortcoming, one might observe an artificially increased number of electrons, which could, in turn, shift the equilibrium Fermi level and increase (decrease) the formation energies (i.e., decrease (increase) the concentration) of negatively (positively) charged defects. Such superfluous electron contributions are avoided with the rigid band shift.

Before describing the results on the defect thermodynamics and kinetics, it is important to note that image charge corrections for charged supercells are scaled with the dielectric constant to include charge screening in the medium. Generally, the electronic dielectric constant is used in scaling because the spurious image charge interaction is screened primarily by a rearrangement of the electronic charge densities. However, in some defect structures, we observe significant structural changes when charges are added to defect structures. This indicates that ionic polarization may also play a role and that the use of $\varepsilon_{\text{static}}$ should also be discussed. Thus, as mentioned before, we evaluated data with both the electronic and the total static dielectric constants. The following procedure is utilized to identify the importance of ionic contributions to ε: (1) the supercell containing the neutral defect is relaxed, (2) the charge is added, and the energy of the structure is calculated without ionic relaxion, (3) the charged structure is ionically relaxed, and (4) the energy difference between the second and the third step is compared to the difference in the Makov−Payne correction using $\varepsilon_{\text{static}}$ and $\varepsilon_{\text{electronic}}$. The energy differences between (2) and (3) were found to vary between 0.04 to 1.9 eV, depending on the defects, which indicates that the contributions of ionic dielectric screening to the Makov−Payne correction are highly variable. Therefore, we present results using both values of the dielectric constant. As described above, DFPT is used to calculate the electronic contribution, and $\varepsilon_{\text{electronic}}$ is obtained as 2.04 for LiF and 1.86 for NaF. Using these values, the monopole corrections are further evaluated as 0.82 (0.78) eV and 3.28 (3.12) eV for 216-atom LiF (NaF) cells with ±1 and ±2 charges. The experimental values of $\varepsilon_{\text{static}}$ are 9.03 for LiF and 5.07 for NaF.[53] The monopole corrections, in this case, are calculated as 0.18 (0.29) eV and 0.74 (1.14) eV for LiF (NaF) cells with ±1 and ±2 charges. In the main text, we primarily present the results obtained using $\varepsilon_{\text{static}}$. In the Supporting Information, detailed results corresponding to $\varepsilon_{\text{electronic}}$ are given. Although these two approaches do result in modest quantitative changes in carrier properties, we note that the general conclusions of the study do not change.

3.2. Defect Thermodynamics in LiF and NaF. We have introduced six types of defects, namely a Li (Na) vacancy (V_{Li} (V_{Na})), a Li (Na) interstitial (Li_i (Na_i)), a Li (Na) Frenkel (vacancy−interstitial) pair (Fp_{Li} (Fp_{Na})), F vacancy (V_F), F interstitial (F_i), and LiF (NaF) Schottky (double-vacancy) pairs (V_{LiF} (V_{NaF})). The formation energies of these defects are evaluated considering various possible charge states (Table 2). Here, we note that the defect pairs (i.e., Frenkel and Schottky) refer to interacting couples such that interstital−vacancy and vacancy−vacancy separations are less than the lattice parameter for the conventional unit cells of LiF and NaF. Several different configurations are investigated by varying defect separation and avoiding cases that may lead to defect recombination/elimination. The lowest energy configurations are found to be associated with the shortest separations, due to a reduction in electrostatic energy with decreasing distance between oppositely-charged defects.

In Figure 2a,b, formation energies of defects, calculated using eq 1, are shown for LiF and NaF at a potential of 0 V on the Li/Li$^+$ (Na/Na$^+$) voltage scales. The figure shows the stability regions for the defects as a function of the Fermi energy. For

Table 2. Evaluated Defects in LiF and NaF and Corresponding Charge States[a]

defect	symbol	charge state
Li (Na) vacancy	V_{Li} (V_{Na})	−2, −1, 0 (″, ′, ×)
Li (Na) interstitial	Li_i (Na_i)	0, 1, 2 (×, •, ••)
Li (Na) Frenkel pair[b]	Fp_{Li} (Fp_{Na})	−1, 0, 1 (′, ×, •)
F vacancy	V_F	−1, 0, 1, 2 (′, ×, •, ••)
F interstitial	F_i	−2, −1, 0 (″, ′, ×)
Schottky defect[b]	V_{LiF} (V_{NaF})	−1, 0, 1 (′, ×, •)

[a] Kroger−Vink representations of the charges are given in parentheses. [b] Frenkel and Schottky defects refer to interacting pairs that are closely spaced.

each defect, only the lowest energy charge state is shown with solid lines. As a first approximation, one could identify the thermodynamic Fermi level from the intersection of the lowest energy charged defects. This intersection, which is in the region highlighted by the gray strip on each plot, is between $V_F^{\bullet}$ and V_{Li}' (V_{Na}'). Because $V_F^{\bullet}$ is less favorable than $V_F^{\times}$ in the highlighted region, $V_F^{\bullet}$ is represented with dotted lines instead of solid lines in Figure 2b. The actual E_F may deviate from this region, however, because the position of the E_F is a function of the concentration of all defects, electrons, and holes. It will later become apparent, by imposing the self-consistent solution to the Fermi level, that the approximation in Figure 2 is accurate in the case of these fluorides. One reason for this result is that the other charge carrying defects have relatively high formation energies, and thus, their contribution to the charge equilibrium is very limited. A second reason is that LiF and NaF have wide band gaps, and the defects favor an E_F close to midgap. Thus, formation of electrons and holes is less likely.

It is seen from Figure 2 that the vacancies of F and Li (Na) are the most stable among the selected defects. The reason for this result is the close-packed nature of rock-salt structure. The interstitials and Frenkel pairs strongly disturb the lattice and increase the energy due to imposed local strains. Consequently, the formation energies of nonvacancy defects are at least 1 eV higher than those of other defects.

It is important to keep in mind that, as briefly discussed above, cation chemical potentials change on the electrodes as the voltage is changed. Thus, the order of defect stability and the location of the Fermi energy also change. The realistic potential window can be considered to be between 0.0 and 0.8 V (which corresponds to first reduction of PC) for anodes in LIBs.[54] Thus, the formation energies presented in Figure 2 are calculated using the chemical potentials of Li and Na in their bulk metallic forms. If the cathode is also considered, this window can further be widened, reaching up to 4 V. In this Li chemical potential range, we again self-consistently solve eq 2 to enforce charge neutrality, and the resulting values of defect formation energies and concentrations are given in Figure 3a,b. As expected, at 0 V vs Li/Li$^+$, the order between the defect formation energies in Figure 3a is the same as the order given at the equilibrium Fermi energy (i.e., within the gray stripe) in Figure 2a. The shift in potential causes new equilibrium conditions at different Fermi levels. From 0 to 4 V, the Fermi level moves ∼4 eV toward the VBM. Consequently, at both limits of μ_{Li}, the calculated Fermi levels are still far away from the band edges. For Li-rich structures (i.e., high μ_{Li}), isolated $V_F^{\bullet}$ and V_{Li}' have the lowest formation energies. A neutral fluorine vacancy is also very close to these two defects. As μ_{Li} decreases, so does the formation energy of $V_F^{\times}$, and $V_{LiF}^{\times}$ becomes the second lowest energy defect. In the whole voltage range, the formation energies and concentrations of $V_F^{\bullet}$ and V_{Li}' are virtually identical, as the charge equilibrium is satisfied by these defects. This couple can also be identified as a Schottky pair composed of noninteracting charged vacancies. Because their formation is interdependent, the formation energy of this type of Schottky defect can simply be evaluated as the sum of formation energies of isolated $V_F^{\bullet}$ and V_{Li}'. When Figure 3c,d is investigated, similar conclusions can be reached for NaF, except that the $V_F^{\times}$ is the lowest energy defect for Na-rich structures. Its formation energy in NaF is slightly smaller compared to LiF. The opposite is true for the $V_{NaF}^{\times}$ defect. As the chemical potential of Na decreases, the formation energy of $V_F^{\times}$ drops below that of isolated $V_F^{\bullet}$ and V_{Na}'. For both LiF and NaF, even the most stable defects have the formation energies between 0.76 and 1.3 eV, rendering their concentrations to be extremely small. As seen in Figures 3b,d, at 0 V vs Li(Na)/Li$^+$(Na$^+$), the highest defect concentrations are on the order of 10^6−10^{10} cm^{-3}, which are 4−8 orders of magnitude lower than the values generally required for defect-mediated processes.

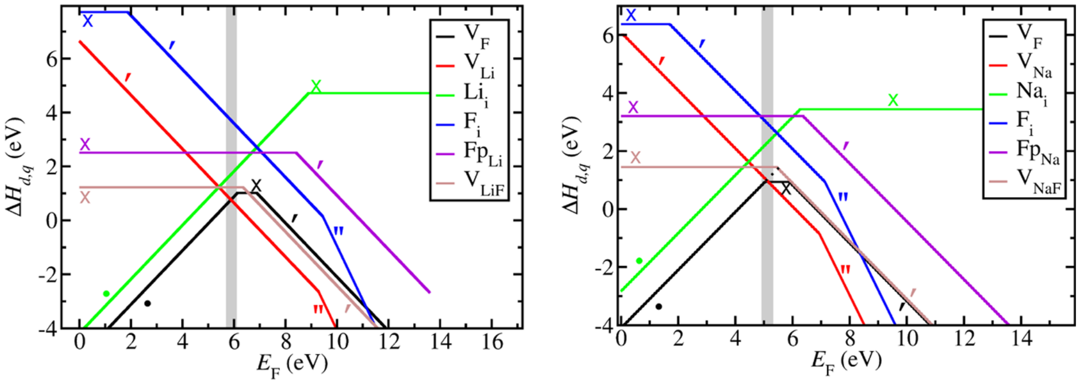

(a) (b)

Figure 2. Formation energies (ΔH) of selected defects in bulk (a) LiF and (b) NaF with respect to the Fermi energy. For a given defect, only the charge state having the lowest ΔH is shown. For identification of defects and their charges, Kroger−Vink notation is used (Table 2). The formation energies are calculated from eq 1, and the chemical potential of Li (Na) is assumed to be that of bulk Li (Na) metal, or 0.0 V on the appropriate reference scales.

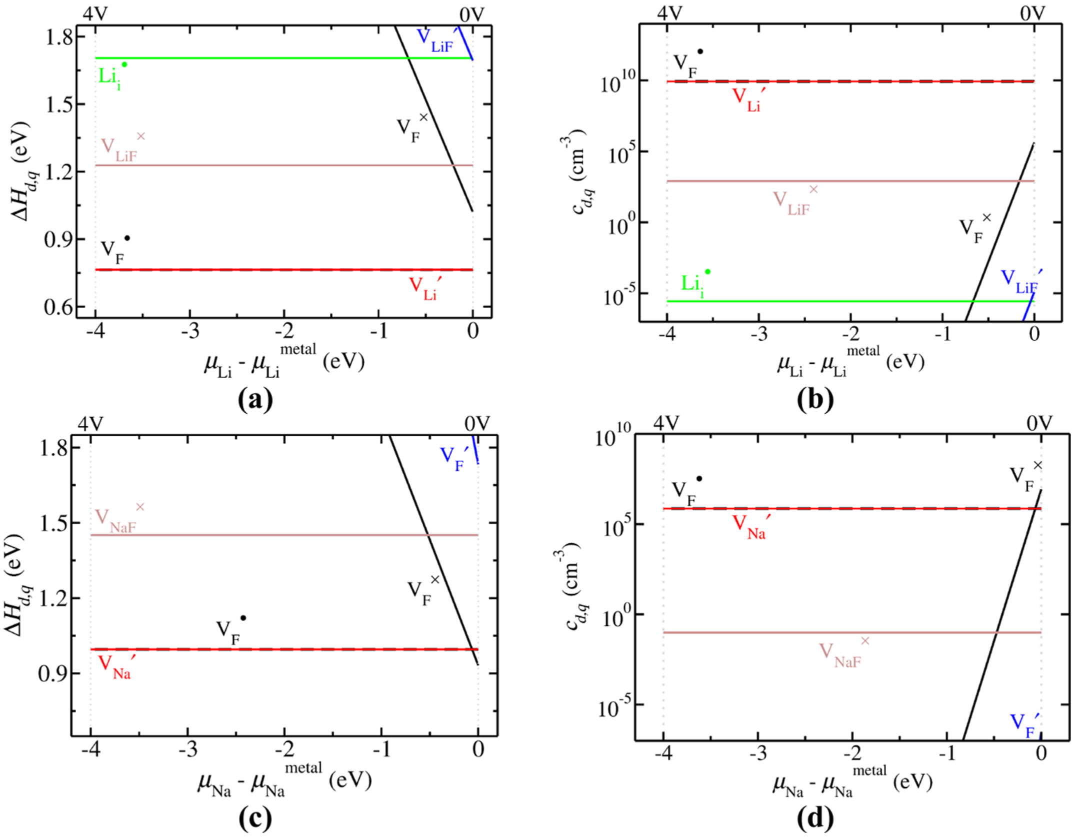

Figure 3. (a and c) Formation energies and (b and d) concentrations of the low energy defects versus cation chemical potential. μ_{Li} and μ_{Na} are referenced to bulk metals. Their limits are shown by vertical dotted lines at 0 and 4 V. The formation energies and concentrations are determined at T = 300 K. See Table 2 for the notation about charge states.

We now compare our results concerning the formation energies of the various defects with the results of available computational and experimental studies. Using empirical potential models, Rowell et al.[55] and Catlow et al.[56] reported Schottky defect formation energies for LiF and NaF in the ranges of 2.37−2.66 eV and 2.91−3.19 eV, respectively. A DFT study[57] predicted the formation energy for the Schottky pair to be in the range of 2.24−2.94 eV, while the defect formation energy for an individual V_{Li}' was reported to be 0.73 eV. Other reported values for Schottky defects are 2.68,[58,59] 2.42,[60] and 2.34−2.68 eV (see ref 62 and references therein) for LiF and 2.42 eV[61] for NaF in an earlier experimental work. Finally, cation vacancy formation was also studied in LiF by Spencer et al.,[62] and a value of 0.73 eV was reported for the formation energy.

In discussing ΔH of Schottky defects, we can give a lower bound and an upper bound corresponding to the formation energies of $V_{Li(Na)F}^{\times}$ and to the isolated $V_F^{\bullet}/V_{Li(Na)}'$ couple (for which the formation energy is $\Delta H_{V_F^{\bullet}} + \Delta H_{V_{Li(Na)}'}$). The reported experimental values generally adapt the convention $c \propto \exp(-E_{experimental}/2kT)$ for the concentration of Schottky defects.[63] From this convention it can be inferred that $2\Delta H_{Schottky} = E_{experimental}$. With this convention, our calculations indicate that the lower and upper bounds, as defined above, are 2.46−3.04 and 2.90−3.98 eV for Schottky defects in LiF and NaF, respectively. The calculated results therefore seem to be on the upper bound of the literature values, but given the inherent uncertainties in the bounds, the agreement is reasonable, particularly for LiF. For the formation energies of lithium cation vacancies, the ΔH of V_{Li}' is obtained as 0.76 eV (see Figure 3a). We note that, if $\varepsilon_{electronic}$ is used, then this value increases to 1.40 eV due to the larger Makov−Payne correction (see Figure S1a in Supporting Information). A good agreement between computations and experimental measurements is therefore achieved by using ε_{static}, but as discussed in section 3.1, some defects might be better described by using $\varepsilon_{electronic}$ (see results in Supporting Information).

Finally, we briefly discuss the impact of higher-level electronic structure corrections on the reported results. In recent years, the use of hybrid functionals has become computationally more accessible, even if such calculations remain 2−3 orders of magnitude slower than LDA or GGA calculations. In some cases, the differences between hybrid and semilocal functional calculations can be quite significant. For instance, Jacobs et al.[64] studied Sc_2O_3 and showed that the use of Heyd−Scuseria−Ernzerhof (HSE) functional instead of GGA can result in a 4 eV change in the defect formation energies. We also refer the reader to a thorough discussion of these issues by Van de Walle and Janotti.[65] To estimate the importance of these effects in LiF and NaF, we performed a limited set of HSE calculations. For these simulations, we used (2 × 2 × 2) supercells. The band gap values obtained from HSE calculations were found to be larger than those of the GGA calculations by about 2 eV, but still lower than the experimental measurements by about 3 eV, for both materials. In addition, we evaluated the formation energies for two defect systems: a positively charged fluorine vacancy and a neutral Schottky defect where lithium and fluorine vacancies are nearest neighbors. When $\Delta E = E_{d,g} - E_0 - \sum_i \mu_i$ is evaluated with both GGA and HSE, we determine that $\Delta E_{HSE} - \Delta E_{GGA}$ is

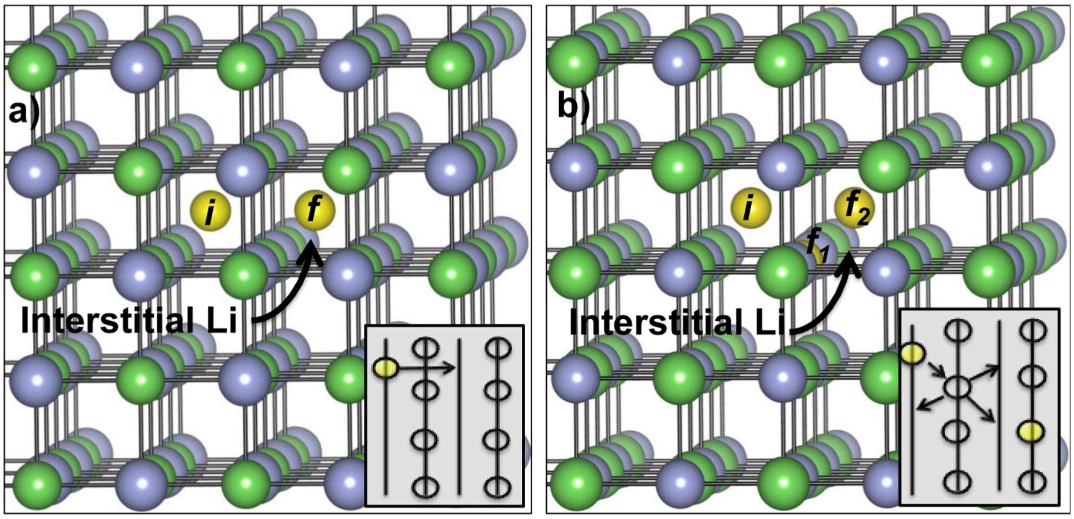

Figure 4. Schematic representations of the diffusion mechanisms for Li interstitials via (a) direct hopping and (b) knock-off mechanism. Gray and green balls represent F and Li, respectively. Yellow balls represent the interstitial Li. The letters i, f_1, and f_2 are the initial and final positions of a Li interstitial for the knock-off mechanism.

Table 3. Diffusion Mechanisms and Associated Barriers (E^b), Diffusion Coefficients ($D_{d,q}$), Defect Concentrations ($c_{d,q}$), and Ionic Conductivities ($\sigma_{d,q}$) of Considered Defects in Bulk LiF and NaF[a]

				$c_{d,q}$ (cm^{-3})			$\sigma_{d,q}$ (S/cm)		
defect	mechanism	$E_{d,q}{}^{b}$ (eV)	$D_{d,q}$ (cm^2/s)	0 V	1 V	4 V	0 V	1 V	4 V
				LiF					
$V_{Li}^{\times}$	vacancy	0.73	2.25×10^{-16}	0	0	0	0	0	0
V_{Li}'	vacancy	0.75	1.04×10^{-16}	1.2×10^{-3}	1.2×10^{-3}	1.2×10^{-3}	4.8×10^{-13}	4.8×10^{-13}	4.8×10^{-13}
$Li_i^{\times}$	direct hopping	0.78	3.25×10^{-17}	0	0	0	0	0	0
$Li_i^{\times}$	knock-off	0.75	1.04×10^{-16}	0	0	0	0	0	0
$V_F^{\times}$	vacancy	1.89	7.32×10^{-36}	3.6×10^{5}	8.3×10^{-12}	0	9.8×10^{-24}	0	0
$V_F^{\bullet}$	vacancy	0.79	2.21×10^{-17}	1.2×10^{-3}	1.2×10^{-3}	1.2×10^{-3}	1.0×10^{-13}	1.0×10^{-13}	1.0×10^{-13}
$V_{LiF}^{\times}$	Li vacancy direct hopping	1.09	2.01×10^{-22}	8.2×10^{2}	8.2×10^{2}	8.2×10^{2}	6.2×10^{-13}	6.2×10^{-13}	6.2×10^{-13}
$V_{LiF}^{\times}$	F vacancy direct hopping	1.10	1.37×10^{-22}	8.2×10^{2}	8.2×10^{2}	8.2×10^{2}	4.2×10^{-13}	4.2×10^{-13}	4.2×10^{-13}
$V_{LiF}^{\times}$	direct hopping (together)	1.09	2.01×10^{-22}	8.2×10^{2}	8.2×10^{2}	8.2×10^{2}	6.2×10^{-13}	6.2×10^{-13}	6.2×10^{-13}
$Li_i^{\bullet}$	direct hopping	0.56	1.61×10^{-13}	2.7×10^{-6}	2.7×10^{-6}	2.7×10^{-6}	1.6×10^{-12}	1.6×10^{-12}	1.6×10^{-12}
$Li_i^{\bullet}$	knock-off	0.27	1.20×10^{-08}	2.7×10^{-6}	2.7×10^{-6}	2.7×10^{-6}	1.2×10^{-7}	1.2×10^{-7}	1.2×10^{-7}
				NaF					
$V_F^{\times}$	vacancy	1.65	2.36×10^{-33}	8.4×10^{6}	1.6×10^{-10}	0	7.4×10^{-20}	1.4×10^{-36}	0
$V_F^{\bullet}$	vacancy	1.11	9.29×10^{-23}	1.4×10^{-11}	1.4×10^{-11}	1.4×10^{-11}	4.8×10^{-27}	4.8×10^{-27}	4.8×10^{-27}
$V_{NaF}^{\times}$	F vacancy direct hopping	1.31	4.05×10^{-26}	9.7×10^{-02}	9.7×10^{-02}	9.7×10^{-02}	1.5×10^{-20}	1.5×10^{-20}	1.5×10^{-20}
$V_{NaF}^{\times}$	Na vacancy direct hopping	1.34	1.27×10^{-26}	9.7×10^{-02}	9.7×10^{-02}	9.7×10^{-02}	4.6×10^{-21}	4.6×10^{-21}	4.6×10^{-21}
V_{Na}'	vacancy	1.08	2.96×10^{-22}	1.4×10^{-11}	1.4×10^{-11}	1.4×10^{-11}	1.5×10^{-26}	1.5×10^{-26}	1.5×10^{-26}
$Na_i^{\bullet}$	knock-off	0.56	1.61×10^{-13}	7.3×10^{-16}	7.3×10^{-16}	7.3×10^{-16}	4.4×10^{-22}	4.4×10^{-22}	4.4×10^{-22}

[a] Concentrations and conductivities are given for the range of alkali chemical potentials at 0−4 V. Concentration values below 10^{-17} cm^{-3} are given as zero. The concentrations of $V_{Li(Na)}'$ and $V_F^{\bullet}$ given in this table are calculated assuming their formation energies are equal to that of a Schottky defect (i.e. made up of isolated vacancies) since in the 0−4 V voltage range formation of $V_{Li(Na)}'$ and $V_F^{\bullet}$ are interdependent. The conductivities of the neutral defects are calculated as if they carry unit charge.

−61 meV for a fluorine vacancy and 117 meV for a Schottky defect. Considering the large absolute values of formation energies for the defects in LiF and NaF, we conclude that the differences between HSE and GGA calculations will not significantly alter our results.

3.3. Diffusion Pathways, Migration Barriers, and Ionic Conductivity in LiF and NaF.

To complete the analysis of ionic conductivities, we calculated the migration barriers for several point defects (both neutral and charged) in LiF and NaF, considering multiple diffusion mechanisms. For LiF, in addition to the diffusion of the vacancy defects, which are the dominant carriers, we also calculated the diffusion barriers of interstitial Li and the vacancy pairs. The possible diffusion mechanisms for the interstitial and vacancy defects in a simple cubic structure of LiF and NaF are limited and much simpler than those in the monoclinic Li_2CO_3 structure.[4] V_{Li}' (V_{Na}') in LiF (NaF) is surrounded by 12 neighboring Li (Na) atoms, which are symmetrically equivalent. Therefore, we have considered only one pathway for the NEB calculations. The V_{Li}' diffuses via a typical direct hopping mechanism in which the position of the vacancy is exchanged with the lattice Li. For the diffusion of the excess Li interstitial (Li_i), the possible

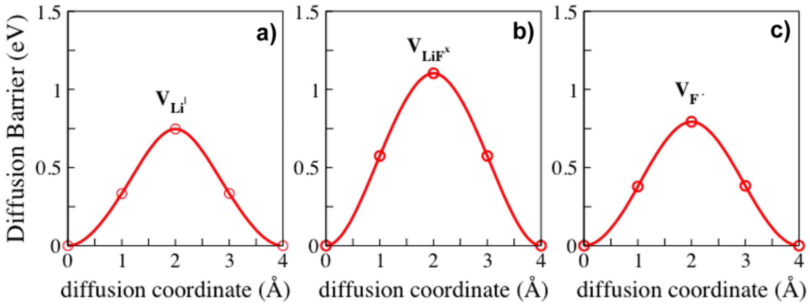

Figure 5. Potential energy profiles of defects via a direct hopping for (a) negatively charged Li vacancy (V_{Li}'), (b) neutral Li−F vacancy couple ($V_{LiF}^{\times}$), and (c) positively charged F vacancy ($V_F^{\bullet}$).

diffusion mechanisms include direct hopping of Li_i onto the next neighboring lattice site (Figure 4a) and diffusion through a repetitive knock-off mechanism in which Li on the lattice sites is displaced (see Figure 4b). In a recent DFT study, the latter mechanism was reported to be the most favorable mechanism of the diffusion carrier ($Li_i^{\bullet}$, positively charged excess interstitial Li ion) in Li_2CO_3, with a lower migration energy than that of direct hopping.[4] The Li−F and Na−F vacancy couples (neutral) are created by removing the neighboring Li/Na and F atoms from bulk LiF and NaF. The diffusion mechanisms that are considered for evaluating the corresponding migration barriers are (1) Li vacancy diffusion via a direct hopping mechanism, (2) F vacancy diffusion via a direct hopping mechanism, (3) Li interstitial via a direct hopping mechanism, (4) Li interstitial via a knock-off mechanism, and (5) diffusion of vacancy pairs via a direct hopping mechanism. The same diffusion mechanisms are considered for NaF.

The calculated migration barriers for all considered defects using the NEB method are given in Table 3, together with the information on the concentration ($c_{d,q}$), associated diffusion coefficients ($D_{d,q}$), and conductivity ($\sigma_{d,q}$). In addition to the diffusion carriers associated with the point defects in each structure, the diffusion barriers for all defect types, including the vacancies, interstitials, and vacancy pair point defects, are included for completeness. In Figure 5, we also present the potential energy profiles obtained using NEB calculations for chosen point defects, namely V_{Li}', $V_{LiF}^{\times}$, and $V_F^{\bullet}$. The results show that for $V_{Li}^{\times}$, the migration barrier is 0.73 eV, which is a very high value for diffusion at room temperature, as reported by an earlier DFT study.[40] Similar to the diffusion barrier for $V_{Li}^{\times}$, we find that the diffusion barrier for V_{Li}' is 0.75 eV. For $Li_i^{\times}$, the diffusion barriers are 0.78 and 0.75 eV for diffusion via a direct hopping and knock-off mechanisms, respectively. In contrast, our calculations suggest that the diffusion barriers for $Li_i^{\bullet}$ are lower than those of the $Li_i^{\times}$ as well as those of the Li vacancies, $V_{Li}^{\times}$, and V_{Li}'. The calculated barriers for $Li_i^{\bullet}$ are 0.56 eV (via direct hopping mechanism) and 0.27 eV (via knock-off mechanism).

The calculated barriers are 1.89 eV for neutral and 0.79 eV for positively charged F vacancies ($V_F^{\bullet}$). The neutral value, in particular, is significantly higher than the corresponding value for Li vacancies. The results of the diffusion barriers for $V_{LiF}^{\times}$ (Li vacancy diffusion, F vacancy diffusion, and Li−F pair simulatenaous diffusion) and $V_{NaF}^{\times}$ (F vacancy and Na vacancy diffusion) via direct hopping show similar migration barriers, which are over 1 eV. On the basis of these values, we conclude that overall diffusion in bulk LiF for dominant defects is very slow. In particular, for the predominant carriers (vacancies), the diffusion barriers are very high at room temperature. The barriers associated with the dominant defects in Li_2CO_3[4,37] and Li_2O[40] are much smaller and comparable with the diffusion barrier in the surface plane of graphite. Thus, diffusion through bulk LiF seems to pose the most severe kinetic limitations among the various inorganic SEI components.

For NaF, the diffusion barriers are calculated for $Na_i^{\bullet}$, V_{Na}', $V_{NaF}^{\times}$, $V_F^{\bullet}$, and $V_F^{\times}$ for vacancy diffusion and diffusion via a knock-off mechanism. Similar to the diffusion barriers calculated in LiF, the barriers for both interstitials and the vacancies are found to be high, hindering diffusion in bulk NaF at room temperature. As with the neutral F vacancy diffusion in LiF, the diffusion barrier for $V_F^{\times}$ in NaF is also found to be the highest (1.65 eV). The Na−F vacancy couple has the second highest diffusion barrier (approximately 1.3 eV), while the negatively charged Na vacancy, V_{Na}', has the third highest diffusion barrier, 1.08 eV. The diffusion barrier for the positively charged Na interstitial, $Na_i^{\bullet}$, via a knock-off mechanism, has the lowest diffusion barrier, as is the case for the $Li_i^{\bullet}$ diffusion barrier in LiF. In comparison with the corresponding diffusion barriers in LiF, however, we find that the barriers calculated in NaF are higher by about 200 meV. As the crystal structures of LiF and NaF are exactly the same (rock salt cubic), the larger Na-ion (70% larger in volume than the Li-ion) in such close-packed crystal structures appears to perturb the lattice to a greater extent and further increasing the barrier for diffusion. These results suggest that the diffusivity in NaF is reduced compared to LiF, and that given the similarity of the defect concentrations, we can expect that the ionic conductivity in NaF will be lower than that of the LiF, as we shall see below.

The results of the diffusion barriers obtained from the NEB calculations can be used to compute the diffusion coefficients for a defect d in the charge state q using the following equation:[66]

$$D_{d,q} = ga^2\nu \exp\left[-\frac{E^{\mathrm{b}}_{d,q}}{k_{\mathrm{B}}T}\right] \tag{5}$$

where $E^{\mathrm{b}}_{d,q}$ is the diffusion barrier associated with defect d, ν is the lattice vibrational frequency, with a typical value of 10^{12} s^{-1}, a is the net distance for a given diffusion process (∼2.03 Å), and g is the dimensionality of the diffusion mechanism (1 or 3). According to the results in section 3.2, the concentration of point defects in LiF and NaF is dilute. Using the self-diffusion coefficients $D_{d,q}$ calculated using the eq 5, and the concentrations $c_{d,q}$ obtained in section 3.2, we can compute the ionic conductivity using the Nernst−Einstein equation:[67]

$$\sigma_{d,q} = D_{d,q}c_{d,q}\frac{q^2F^2}{RT} \tag{6}$$

where q is the ion's charge, F is Faraday's constant, R is the gas constant, T is the temperature (300 K), $D_{d,q}$ is the diffusion coefficient of defect d at a given temperature T, and $c_{d,q}$ is the concentration of the defect d.

For LiF, the results of the diffusion coefficients ($D_{d,q}$), the barriers ($E^{b}{}_{d,q}$), the concentrations ($c_{d,q}$), and the conductivities ($\sigma_{d,q}$) are reported in Table 3 at 300 K and various voltages in the anode−cathode range. When $\varepsilon_{\text{static}}$ is used for Makov−Payne corrections, the results for the low voltage regime (0 to 1 V) suggest that $\text{Li}_i^{\bullet}$ dominates the ionic conduction. Although the concentration of the lithium interstitial is lower than the concentrations of $V_{\text{LiF}}^{\times}$ and $V_F^{\bullet}$, the diffusion barrier for the $\text{Li}_i^{\bullet}$ knock-off mechanism is lower than that of any other transport process. This low barrier leads to a six orders of magnitude higher ionic conductivity for $\text{Li}_i^{\bullet}$ compared to the Schottky defect. Individual V_{Li}' and $V_F^{\bullet}$ formation energies are about 0.76 eV. However, their concentrations must be equal in order to maintain charge neutrality. Thus, the actual concentration of these defects can be found from the sum of their formation energies, which significantly reduces their concentration, as given in Table 3.

We now turn to the results obtained for high voltages (4 V) and analyze the possible changes in the dominant carriers in bulk LiF (Table 3). The analysis of the formation energies and the defect concentrations shows that, except for the neutral Li and F vacancies ($V_{\text{Li}}^{\times}$, $V_F^{\times}$), there are no changes in the concentration of the defects. At 4 V, we find that the concentration of $V_{\text{Li}}^{\times}$ is significantly increased, while the $V_F^{\times}$ concentration is lowered. These results therefore suggest that the dominant contribution to the ionic conductivities at this high voltage will still be from $\text{Li}_i^{\bullet}$, similar to what is identified at the low voltage regime (0−1 V).

As compared to LiF, the conductivity from defect carriers in NaF at low voltages (0−1 V) is very small (varying from 10^{-20} to 10^{-36} S/cm). The diffusion barrier for the $\text{Na}_i^{\bullet}$ via a knock-off mechanism is two times that of $\text{Li}_i^{\bullet}$. Consequently, the $\text{Na}_i^{\bullet}$ contribution to ionic conductivity is not the dominant one. The Na−F vacancy couple ($V_{\text{NaF}}^{\times}$), and the neutral F vacancy, are the main carriers driving the ionic motion at low voltages. At high voltage (4 V), on the other hand, the concentration of $V_F^{\times}$ is very low, and this reduces its contribution to the ionic conductivity. The primary carrier in this regime is only $V_{\text{NaF}}^{\times}$. We should, however, note that the ionic conductivity is still very low, in the 10^{-20} S/cm range, as compared to that in LiF, 10^{-7} S/cm. The higher formation energies and diffusion barriers in NaF can be explained by its slightly higher ionic character and lower dielectric constant, which reduce the medium's ability to screen charges. The experimental melting temperature (which is related to the vacancy formation energies) of NaF is also higher than that of LiF,[68] indicating a similar qualitative ordering between defect formation energies as is found in the calculations.

As previously mentioned, we also present the ionic conductivities of defects when $\varepsilon_{\text{electronic}}$ is used in the monopole correction in Table S1 (Supporting Information). One main difference between Table 3 and Table S1 is the contribution of the positively charged Li interstitial to the conductivity of LiF. Scaling the monopole term with a smaller dielectric constant gives a larger correction value, and the formation energy of $\text{Li}_i^{\bullet}$ is therefore increased to a degree that it is not important for ionic conductivity. Another important difference is the decoupling of V_{Na}' and $V_F^{\bullet}$, as the chemical potential of Na decreases in NaF, which is observed in calculations utilizing $\varepsilon_{\text{electronic}}$, as seen in Figures S1 and S2. This decoupling is caused by excited holes in the valence band allowing more V_{Na}' to be present. The holes are generated with similar concentrations to the $V_{\text{Na}}'/V_F^{\bullet}$ couple since the Fermi level is close enough to the VBM. For neutral defects, the Makov−Payne term is not relevant, so their ionic conductivities are the same. In the end, it is worth mentioning that, although some differences exist in the formation energies of charged defects between utilizing $\varepsilon_{\text{static}}$ and $\varepsilon_{\text{electronic}}$, our main conclusions on the magnitudes of ionic conductivity in LiF and NaF are unchanged.

The features of defect chemistry in LiF, discussed above, agree well with the general discussions in the literature. Indeed, the defect chemistry of LiF has been reported to be rather simple, characterized by Schottky disorder with a significant ionic gap corresponding to intrinsically low carrier densities of Li and F vacancies (V_{Li}' and $V_F^{\bullet}$).[60] The results obtained in our study regarding the mobility and concentration of Li and F vacancies correspond well with these earlier experimental reports. The small concentrations of these intrinsic defects could raise the question of whether extrinsic defects play a vital role in LiF and NaF. For instance, other cations of higher valence can lead to additional Li or Na vacancies. In fact, during the operation of the battery, some cations can dissolve into the electrolyte and deposit in SEI compounds. An important example of cation dissolution and crossover is Mn. To assess the effects on defect thermodynamics of Mn substitution in LiF, we consider two more defects, namely, single Mn substitution (neutral and +1 charge states) and Mn substitution-Li vacancy couple (neutral charge state) in our self-consistent formation energy calculation. Again, a 216-atom supercell is used. We use two possible references for manganese: bulk Mn metal, or MnF_2, which may form on the anode. It is seen that at the metallic Mn limit, Mn substitutions are highly unfavorable (1.8 eV), and the formation energies of all native defects remain unchanged, whereas at the chemical potential limit where MnF_2 is stable, the formation energy of V_{Li}' can be reduced to 0.63 eV with Mn substitution. The total formation energy for the Mn substitution/Li vacancy couple will be 1.26 eV, which is still too high to obtain appreciable vacancy concentrations. Nevertheless, it is worth investigating the effect of other possible cations in batteries in future studies. Apart from naturally occurring SEI, "artificial SEI" precoatings may be considered for electrode protection. In this case, it is possible to synthesize and engineer LiF or NaF coatings by introducing higher valence cations, such as via ion implantation. This process can artificially increase the concentrations of Li and Na vacancies beyond the equilibrium levels, which can significantly increase the ionic conductivity of the coatings.

In addition, it is worth pointing out that the conductivity and carrier characteristics of LiF/NaF thin films or interfaces could differ significantly from that of bulk systems. An experimental study by Li et al.[69] on the charge carrier accumulation in LiF due to Li ion absorption at the LiF/TiO_2 interface suggested that as far as LiF is concerned, Li^+ deficiency is easily feasible but not Li^+ excess. The authors showed, for the expected space charge effect of the LiF/TiO_2 interface, that Li^+ transfer from LiF to TiO_2 should lead to an accumulation of Li interstitials ($\text{Li}_i^{\bullet}$) on the TiO_2 side, while Li vacancies (V_{Li}') should be accumulated on the LiF side. By varying the thickness of the LiF film, they showed that the thinner sample has higher conductivity, which is attributed to ionic carrier accumulation (mainly V_{Li}') at LiF/TiO_2 interface. A conductivity as high as

10^{-6} S/cm was achieved for an 80 nm thick LiF thin film at 190 °C. A comparative experimental study of LiF thin films on various oxide substrates for elucidating the interfacial defect chemistry reported enormous richness of interfacial defect chemistry, and its relevance for the overall material properties. The conductivities were strongly influenced by glass/ceramic interfaces.[70]

On the basis of these interesting experimental observations, we close by suggesting that it is worthwhile to further investigate defect chemistry and mobility in both thin LiF and NaF films. In such future studies, the development of a detailed understanding of ion transport via grain boundaries and at the interfaces between LiF and NaF and the electrode surface will provide an even more complete understanding of transport through these fascinating components of the SEI.

4. CONCLUSIONS

We report on extensive DFT calculations to characterize the role of two isostructural compounds, LiF and NaF, in cation transport through the SEI in lithium ion and sodium ion batteries. To understand the transport process, we calculate the concentration of point defects that can facilitate diffusion. Defect formation energies in the range of possible Li (Na) chemical potentials on the anode and cathode are obtained by self-consistently solving the charge equilibrium equation. The computations show that vacancies are the lowest energy defects in both compounds, possibly due to their ionic close packing. Regardless of the type of vacancy, however, we find that the lowest defect formation energies are around 0.76 eV. Thus, the defect concentrations are orders of magnitude smaller than the scales that are generally relevant for defect engineering in bulk structures.

Considering both neutral and charged defects, including vacancies, Li(Na) interstitials, and Li−F and Na−F pairs, we calculate activation barriers for diffusion via vacancy, direct hopping, and knock-off mechanisms. In most cases, we observe that the diffusion barriers in both LiF and NaF are very high, ranging from ∼0.7 to 2.0 eV, with the barriers for NaF being slightly higher than LiF. This suggests that the diffusion in these inorganic SEI compounds presents kinetic limitations and potentially affects the rate performance of the battery. One exception to this conclusion is the Li interstitial diffusion through a knock-off mechanism, for which the transport barrier is calculated as 0.27 eV. For LiF, the contributions to the ionic conductivity from the considered defects are found to be on the order of $\sim 10^{-7}-10^{-13}$ S/cm. These trends are very similar at voltages characteristic of the cathode. On the other hand, for NaF, the ionic conductivity is many orders of magnitude lower in comparison with that of LiF. Under cathode conditions, the order of conductivity is not changed significantly and the overall ionic conductivity is still very low. In general, the reported conductivities in both LiF and NaF are significantly lower than corresponding reports in Li_2CO_3. This comparison highlights the fact that the inorganic compounds making up the SEI layer vary dramatically in their ionic conductivities. Thus, it may be possible to optimize ion transport through SEI compounds by carefully controlling the near-surface heterostructures. We further suggest that additional analysis regarding the diffusion in ultrathin films of LiF and NaF could be potentially useful for providing further understanding of the kinetics in these inorganic SEI compounds.

■ ASSOCIATED CONTENT

Supporting Information

The Supporting Information is available free of charge on the ACS Publications website at DOI: 10.1021/acsami.5b02904.

> Selection of dielectric constant for the Makov−Payne correction; plots of formation energy and concentration versus chemical potential for LiF and NaF using the electronic dielectric constants; diffusion mechanisms and barriers, diffusion coefficients, defect concentrations, and ionic conductivities for all the defects in bulk LiF and NaF using the electronic dielectric constants. (PDF)

■ AUTHOR INFORMATION

Corresponding Author

*E-mail: jgreeley@purdue.edu.

Author Contributions

[§]These authors contributed equally to the work.

Notes

The authors declare no competing financial interest.

■ ACKNOWLEDGMENTS

This research was supported as part of the Center for Electrochemical Energy Science, an Energy Frontier Research Center funded by the U.S. Department of Energy, Office of Science, Office of Basic Energy Sciences. Use of the Center for Nanoscale Materials was supported by the U.S. Department of Energy, Office of Science, Office of Basic Energy Sciences, under Contract No. DE-AC02-06CH11357. Some calculations were performed at the National Energy Research Scientific Computing Center (NERSC). We also gratefully acknowledge the computing resources provided on Blues and Fusion, high-performance computing clusters operated by the Laboratory Computing Resource Center at Argonne National Laboratory.

■ REFERENCES

(1) Dunn, B.; Kamath, H.; Tarascon, J. M. Electrical Energy Storage for the Grid: A Battery of Choices. *Science* **2011**, *334* (6058), 928−935.

(2) Slater, M. D.; Kim, D.; Lee, E.; Johnson, C. S. Sodium-Ion Batteries. *Adv. Funct. Mater.* **2013**, *23* (8), 947−958.

(3) Wang, Y.; Balbuena, P. B. *Lithium-Ion Batteries: Solid-Electrolyte Interphase*. Imperial College: London, 2004.

(4) Shi, S.; Lu, P.; Liu, Z.; Qi, Y.; Hector, L. G., Jr.; Li, H.; Harris, S. J. Direct Calculation of Li-ion Transport in the Solid Electrolyte Interphase. *J. Am. Chem. Soc.* **2012**, *134* (37), 15476−87.

(5) Tavassol, H.; Buthker, J. W.; Ferguson, G. A.; Curtiss, L. A.; Gewirth, A. A. Solvent Oligomerization during SEI Formation on Model Systems for Li-Ion Battery Anodes. *J. Electrochem. Soc.* **2012**, *159* (6), A730−A738.

(6) Tasaki, K.; Harris, S. J. Computational Study on the Solubility of Lithium Salts Formed on Lithium Ion Battery Negative Electrode in Organic Solvents. *J. Phys. Chem. C* **2010**, *114* (17), 8076−8083.

(7) Ponrouch, A.; Marchante, E.; Courty, M.; Tarascon, J.-M.; Palacín, M. R. In Search of an Optimized Electrolyte for Na-Ion Batteries. *Energy Environ. Sci.* **2012**, *5* (9), 8572−8583.

(8) Aurbach, D.; Ein-Eli, Y.; Chusid, O.; Carmeli, Y.; Babai, M.; Yamin, H. The Correlation Between the Surface Chemistry and the Performance of Li-Carbon Intercalation Anodes for Rechargeable 'Rocking-Chair' Type Batteries. *J. Electrochem. Soc.* **1994**, *141* (3), 603−611.

(9) Arora, P.; White, R. E.; Doyle, M. Capacity Fade Mechanisms and Side Reactions in Lithium-Ion Batteries. *J. Electrochem. Soc.* **1998**, *145* (10), 3647−3667.

(10) Aurbach, D. Review of Selected Electrode-Solution Interactions which Determine the Performance of Li and Li Ion Batteries. *J. Power Sources* **2000**, *89* (2), 206−218.

(11) Aurbach, D.; Markovsky, B.; Weissman, I.; Levi, E.; Ein-Eli, Y. On the Correlation Between Surface Chemistry and Performance of Graphite Negative Electrodes for Li Ion Batteries. *Electrochim. Acta* **1999**, *45* (1−2), 67−86.

(12) Deshpande, R.; Verbrugge, M.; Cheng, Y. T.; Wang, J.; Liu, P. Battery Cycle Life Prediction with Coupled Chemical Degradation and Fatigue Mechanics. *J. Electrochem. Soc.* **2012**, *159* (10), A1730−A1738.

(13) Vetter, J.; Novák, P.; Wagner, M. R.; Veit, C.; Möller, K. C.; Besenhard, J. O.; Winter, M.; Wohlfahrt-Mehrens, M.; Vogler, C.; Hammouche, A. Ageing Mechanisms in Lithium-Ion Batteries. *J. Power Sources* **2005**, *147* (1−2), 269−281.

(14) Andersson, A. M.; Abraham, D. P.; Haasch, R.; MacLaren, S.; Liu, J.; Amine, K. Surface Characterization of Electrodes from High Power Lithium-Ion Batteries. *J. Electrochem. Soc.* **2002**, *149* (10), A1358−A1369.

(15) Andersson, A. M.; Edstrom, K. Chemical Composition and Morphology of the Elevated Temperature SEI on Graphite. *J. Electrochem. Soc.* **2001**, *148* (10), A1100−A1109.

(16) Komaba, S.; Murata, W.; Ishikawa, T.; Yabuuchi, N.; Ozeki, T.; Nakayama, T.; Ogata, A.; Gotoh, K.; Fujiwara, K. Electrochemical Na Insertion and Solid Electrolyte Interphase for Hard-Carbon Electrodes and Application to Na-Ion Batteries. *Adv. Funct. Mater.* **2011**, *21* (20), 3859−3867.

(17) Xu, K.; Zhuang, G. V.; Allen, J. L.; Lee, U.; Zhang, S. S.; Ross, P. N., Jr.; Jow, T. R. Syntheses and Characterization of Lithium Alkyl Mono- and Dicarbonates as Components of Surface Films in Li-Ion Batteries. *J. Phys. Chem. B* **2006**, *110* (15), 7708−7719.

(18) Nie, M. Y.; Chalasani, D.; Abraham, D. P.; Chen, Y. J.; Bose, A.; Lucht, B. L. Lithium Ion Battery Graphite Solid Electrolyte Interphase Revealed by Microscopy and Spectroscopy. *J. Phys. Chem. C* **2013**, *117* (3), 1257−1267.

(19) Wang, C.; Kakwan, I.; Appleby, A. J.; Little, F. E. In Situ Investigation of Electrochemical Lithium Intercalation into Graphite Powder. *J. Electroanal. Chem.* **2000**, *489* (1−2), 55−67.

(20) Verma, P.; Maire, P.; Novak, P. A Review of the Features and Analyses of the Solid Electrolyte Interphase in Li-Ion Batteries. *Electrochim. Acta* **2010**, *55* (22), 6332−6341.

(21) Arreaga-Salas, D. E.; Sra, A. K.; Roodenko, K.; Chabal, Y. J.; Hinkle, C. L. Progression of Solid Electrolyte Interphase Formation on Hydrogenated Amorphous Silicon Anodes for Lithium-Ion Batteries. *J. Phys. Chem. C* **2012**, *116* (16), 9072−9077.

(22) Aurbach, D.; Gamolsky, K.; Markovsky, B.; Salitra, G.; Gofer, Y.; Heider, U.; Oesten, R.; Schmidt, M. The Study of Surface Phenomena Related to Electrochemical Lithium Intercalation into Li_xMO_y Host Materials (M = Ni, Mn). *J. Electrochem. Soc.* **2000**, *147* (4), 1322−1331.

(23) Ufheil, J.; Wursig, A.; Schneider, O. D.; Novak, P. Acetone as Oxidative Decomposition Product in Propylene Carbonate Containing Battery Electrolyte. *Electrochem. Commun.* **2005**, *7* (12), 1380−1384.

(24) Moshkovich, M.; Cojocaru, M.; Gottlieb, H. E.; Aurbach, D. The Study of the Anodic Stability of Alkyl Carbonate Solutions by in Situ FTIR Spectroscopy, EQCM, NMR and MS. *J. Electroanal. Chem.* **2001**, *497* (1−2), 84−96.

(25) Matsuta, S.; Kato, Y.; Ota, T.; Kurokawa, H.; Yoshimura, S.; Fujitani, S. Electron-Spin-Resonance Study of the Reaction of Electrolytic Solutions on the Positive Electrode for Lithium-Ion Secondary Batteries. *J. Electrochem. Soc.* **2001**, *148* (1), A7−A10.

(26) Yang, L.; Ravdel, B.; Lucht, B. L. Electrolyte Reactions with the Surface of High Voltage $LiNi_{0.5}Mn_{1.5}O_4$ Cathodes for Lithium-Ion Batteries. *Electrochem. Solid-State Lett.* **2010**, *13* (8), A95−A97.

(27) Churikov, A. V. Transfer Mechanism in Solid-Electrolyte Layers on Lithium: Influence of Temperature and Polarization. *Electrochim. Acta* **2001**, *46* (15), 2415−2426.

(28) Peled, E. The Electrochemical Behavior of Alkali and Alkaline Earth Metals in Nonaqueous Battery Systems-The Solid Electrolyte Interphase Model. *J. Electrochem. Soc.* **1979**, *126* (12), 2047−2051.

(29) Borodin, O.; Smith, G. D. LiTFSI Structure and Transport in Ethylene Carbonate from Molecular Dynamics Simulations. *J. Phys. Chem. B* **2006**, *110* (10), 4971−7.

(30) Wang, Y. X.; Balbuena, P. B. Combined Ab Initio Quantum Mechanics and Classical Molecular Dynamics Studies of Polyphosphazene Polymer Electrolytes: Competitive Solvation of Li+ and $LiCF_3SO_3$. *J. Phys. Chem. B* **2004**, *108* (40), 15694−15702.

(31) Ganesh, P.; Jiang, D. E.; Kent, P. R. Accurate Static and Dynamic Properties of Liquid Electrolytes for Li-Ion Batteries from Ab Initio Molecular Dynamics. *J. Phys. Chem. B* **2011**, *115* (12), 3085−90.

(32) Sutjianto, A.; Curtiss, L. A. Li+-Diglyme Complexes: Barriers to Lithium Cation Migration. *J. Phys. Chem. A* **1998**, *102* (6), 968−974.

(33) Johansson, P.; Jacobsson, P. Rational Design of Electrolyte Components by Ab Initio Calculations. *J. Power Sources* **2006**, *153* (2), 336−344.

(34) Van der Ven, A.; Ceder, G. Lithium Diffusion in Layered Li_xCoO_2. *Electrochem. Solid-State Lett.* **1999**, *3* (7), 301−304.

(35) Hao, S.; Wolverton, C. Lithium Transport in Amorphous Al_2O_3 and AlF_3 for Discovery of Battery Coatings. *J. Phys. Chem. C* **2013**, *117* (16), 8009−8013.

(36) Iddir, H.; Curtiss, L. A. Li Ion Diffusion Mechanisms in Bulk Monoclinic Li_2CO_3 Crystals from Density Functional Studies. *J. Phys. Chem. C* **2010**, *114* (48), 20903−20906.

(37) Shi, S. Q.; Qi, Y.; Li, H.; Hector, L. G. Defect Thermodynamics and Diffusion Mechanisms in Li_2CO_3 and Implications for the Solid Electrolyte Interphase in Li-Ion Batteries. *J. Phys. Chem. C* **2013**, *117* (17), 8579−8593.

(38) Herstedt, M.; Stjerndahl, M.; Gustafsson, T.; Edstrom, K. Anion Receptor for Enhanced Thermal Stability of the Graphite Anode Interface in a Li-Ion Battery. *Electrochem. Commun.* **2003**, *5* (6), 467−472.

(39) Koyama, Y.; Yamada, Y.; Tanaka, I.; Nishitani, S. R.; Adachi, H.; Murayama, M.; Kanno, R. Evaluation of Migration Energy of Lithium Ions in Chalcogenides and Halides by First Principles Calculation. *Mater. Trans.* **2002**, *43* (7), 1460−1463.

(40) Chen, Y. C.; Ouyang, C. Y.; Song, L. J.; Sun, Z. L. Electrical and Lithium Ion Dynamics in Three Main Components of Solid Electrolyte Interphase from Density Functional Theory Study. *J. Phys. Chem. C* **2011**, *115* (14), 7044−7049.

(41) Maier, J. Defect Chemistry: Composition, Transport, and Reactions in the Solid State; Part I: Thermodynamics. *Angew. Chem., Int. Ed. Engl.* **1993**, *32* (3), 313−335.

(42) Kresse, G.; Furthmuller, J. Efficient Iterative Schemes for Ab Initio Total-Energy Calculations Using a Plane-Wave Basis Set. *Phys. Rev. B* **1996**, *54* (16), 11169−11186.

(43) Perdew, J. P.; Burke, K.; Ernzerhof, M. Generalized Gradient approximation Made Simple. *Phys. Rev. Lett.* **1996**, *77* (18), 3865−3868.

(44) Leslie, M.; Gillan, M. J. The Energy and Elastic Dipole Tensor of Defects in Ionic-Crystals Calculated by the Supercell Method. *J. Phys. C: Solid State Phys.* **1985**, *18* (5), 973−982.

(45) Sun, R.; Chan, M. K. Y.; Kang, S.; Ceder, G. Intrinsic Stoichiometry and Oxygen-Induced p-type Conductivity of Pyrite FeS_2. *Phys. Rev. B* **2011**, *84* (3), 035212−7.

(46) Makov, G.; Payne, M. C. Periodic Boundary Conditions in *Ab Initio* Calculations. *Phys. Rev. B* **1995**, *51* (7), 4014−4022.

(47) Van de Walle, C. G.; Neugebauer, J. First-Principles Calculations for Defects and Impurities: Applications to III-Nitrides. *J. Appl. Phys.* **2004**, *95* (8), 3851−3879.

(48) Lin, S.-k.; Yeh, C.-k.; Puchala, B.; Lee, Y.-L.; Morgan, D. Ab Initio Energetics of Charge Compensating Point Defects: A Case Study on MgO. *Comput. Mater. Sci.* **2013**, *73* (0), 41−55.

(49) Sheppard, D.; Terrell, R.; Henkelman, G. Optimization Methods for Finding Minimum Energy Paths. *J. Chem. Phys.* **2008**, *128* (13), 134106−10.

(50) Klimes, J.; Bowler, D. R.; Michaelides, A. Van der Waals Density Functionals Applied to Solids. *Phys. Rev. B* **2011**, *83* (19), 195131.

(51) Roy, G.; Singh, G.; Gallon, T. E. The Electron Energy Loss Spectra of Some Alkali Halides in the Band Gap Region. *Surf. Sci.* **1985**, *152–153*, 1042–1050.

(52) Marques, M. A. L.; Vidal, J.; Oliveira, M. J. T.; Reining, L.; Botti, S. Density-Based Mixing Parameter for Hybrid Functionals. *Phys. Rev. B* **2011**, *83* (3), 035119.

(53) Andeen, C.; Fontanella, J.; Schuele, D. Low-Frequency Dielectric Constant of LiF, NaF, NaCl, NaBr, KCl, and KBr by the Method of Substitution. *Phys. Rev. B* **1970**, *2* (12), 5068–5073.

(54) Verbrugge, M. W.; Baker, D. R.; Koch, B. J. Mathematical Modeling of High-Power-Density Insertion Electrodes for Lithium Ion Batteries. *J. Power Sources* **2002**, *110* (2), 295–309.

(55) Rowell, D. K.; Sangster, M. J. L. Calculations of Intrinsic Defect Energies in the Alkali-Halides. *J. Phys. C: Solid State Phys.* **1981**, *14* (21), 2909–2921.

(56) Catlow, C. R. A.; Corish, J.; Diller, K. M.; Jacobs, P. W. M.; Norgett, M. J. The Contribution of Vacancy Defects to Mass Transport in Alkali Halides-an Assessment Using Theoretical Calculations of Defect Energies. *J. Phys. C: Solid State Phys.* **1979**, *12* (3), 451–464.

(57) Pan, J.; Cheng, Y.-T.; Qi, Y. General Method to Predict Voltage-Dependent Ionic Conduction in a Solid Electrolyte Coating on Electrodes. *Phys. Rev. B* **2015**, *91* (13), 134116.

(58) Pizzini, S. Ionic Conductivity in Lithium Compounds. *J. Appl. Electrochem.* **1971**, *1* (3), 153–161.

(59) Haven, Y. The Ionic Conductivity of Li-Halide Crystals. *Recl. Trav. Chim. Pays-Bas* **1950**, *69* (12), 1471–1489.

(60) Stoebe, T. G.; Huggins, R. A. Measurement of Ionic Diffusion in Lithium Fluoride by Nuclear Magnetic Resonance Techniques. *J. Mater. Sci.* **1966**, *1* (2), 117–126.

(61) Bauer, C. F.; Whitmore, D. H. Ionic Conductivity of Sodium fluoride. *Phys. Status Solidi B* **1970**, *37* (2), 585–598.

(62) Spencer, O. S.; Plint, C. A. Formation Energy of Individual Cation Vacancies in LiF and NaCl. *J. Appl. Phys.* **1969**, *40* (1), 168–172.

(63) Dreyfus, R. W.; Nowick, A. S. Ionic Conductivity of Doped NaCl Crystals. *Phys. Rev.* **1962**, *126* (4), 1367–1377.

(64) Jacobs, R. M.; Booske, J. H.; Morgan, D. Intrinsic Defects and Conduction Characteristics of Sc_2O_3 in Thermionic Cathode Systems. *Phys. Rev. B* **2012**, *86* (5), 054106.

(65) Van de Walle, C. G.; Janotti, A. Advances in Electronic Structure Methods for Defects and Impurities in Solids. *Phys. Status Solidi B* **2011**, *248* (1), 19–27.

(66) Van der Ven, A.; Ceder, G.; Asta, M.; Tepesch, P. D. First-Principles Theory of Ionic Diffusion with Nondilute Carriers. *Phys. Rev. B* **2001**, *64* (18), 184307–17.

(67) Birks, N.; Meier, G. H. *Introduction to High Temperature Oxidation of Metals*. Edward Arnold Publishers: London, 1983.

(68) Sirdeshmukh, D. B.; Sirdeshmukh, L.; Subhadra, K. G. *Alkali Halides: A Handbook of Physical Properties*. Springer: New York, 2001.

(69) Li, C.; Gu, L.; Guo, X.; Samuelis, D.; Tang, K.; Maier, J. Charge Carrier Accumulation in Lithium Fluoride Thin Films due to Li-Ion Absorption by Titania (100) Subsurface. *Nano Lett.* **2012**, *12* (3), 1241–1246.

(70) Li, C.; Maier, J. Ionic Space Charge Effects in Lithium Fluoride Thin Films. *Solid State Ionics* **2012**, *225*, 408–411.